NANO LETTERS

Letter

pubs.acs.org/NanoLett

Bottom-up Approach toward Single-Crystalline VO_2-Graphene Ribbons as Cathodes for Ultrafast Lithium Storage

Shubin Yang,*[†] Yongji Gong,[‡] Zheng Liu,[†] Liang Zhan,[†] Daniel P. Hashim,[†] Lulu Ma,[†] Robert Vajtai,[†] and Pulickel M. Ajayan*[†,‡]

[†]Department of Mechanical Engineering & Materials Science, Rice University, Houston, Texas 77005, United States

[‡]Department of Chemistry, Rice University, Houston, Texas 77005, United States

S *Supporting Information*

ABSTRACT: Although lithium ion batteries have gained commercial success owing to their high energy density, they lack suitable electrodes capable of rapid charging and discharging to enable a high power density critical for broad applications. Here, we demonstrate a simple bottom-up approach toward single crystalline vanadium oxide (VO_2) ribbons with graphene layers. The unique structure of VO_2-graphene ribbons thus provides the right combination of electrode properties and could enable the design of high-power lithium ion batteries. As a consequence, a high reversible capacity and ultrafast charging and discharging capability is achieved with these ribbons as cathodes for lithium storage. A full charge or discharge is capable in 20 s. More remarkably, the resulting electrodes retain more than 90% of the initial capacity after cycling more than 1000 times at an ultrahigh rate of 190C, providing the best reported rate performance for cathodes in lithium ion batteries to date.

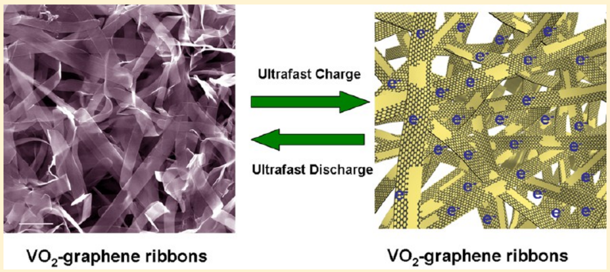

KEYWORDS: *Nanoribbons, graphene, ultrafast, electrode, lithium ion batteries*

Lithium ion batteries are integral power sources in several of today's technologies.[1−8] The achievement of high-rate capability, most important for high power density applications such as in electric vehicles, is known to be hindered by kinetic problems involving slow ion and electron diffusions in the electrode materials.[9,10] An effective strategy to enhance current rates is by reducing the characteristic dimensions of the electrochemically active materials, since the diffusion time of lithium ions (t) is proportional to the square of the diffusion length (L) ($t \approx L^2/D$).[10,11] In this regard, numerous nanoscale materials including nanowires,[12] nanotubes,[3,13] nanoparticles,[14−16] nanosheets,[17,18] and nanoribbons[19,20] have been recently synthesized and demonstrated for improving electrochemical performance for lithium storage. However, only modest improvements in rate performances have been observed[10,21] due to difficulties to simultaneously possess efficient ion and electron pathways in unmodified nanomaterials.[1,9] To further circumvent this problem, various three-dimensional (3D) architectures with high electrical conductivity have been employed to serve as current collectors for nanomaterials.[21−23] Although some improvements in charging and discharging rates have been achieved with minimal capacity loss,[9] these architectures commonly lead to the high-weight fraction of current collectors in electrodes, decreasing the overall energy density of batteries. Moreover, the complicated and limited approaches to fabricate such 3D architectures largely hamper their practical applications in lithium ion batteries.[9,21]

Here, we demonstrate a simple bottom-up approach for synthesizing vanadium dioxide (VO_2) ribbons with thin, flexible, single-crystalline features simultaneously included with graphene layers as building blocks to construct 3D architectures (denoted as VO_2-graphene architecture) (Figures 1 and S1). Such unique architectures can provide (1) numerous channels for the access of electrolyte—facilitating rapid diffusion of lithium ions within the electrode material, (2) a short solid-state diffusion length for lithium—owing to the thin nature of VO_2 ribbons, (3) a high electrical conductivity of the overall electrode—based on the graphene network, and (4) the highest content of elelctrochemically active material within the electrode (up to 84% by weight). Our architectures can satisfy all of the kinetic requirements for ultrafast charging and discharging of an ideal electrode material, that is, rapid ion and electron diffusions. As a consequence, the VO_2-graphene architectures enable ultrafast, supercapacitor-like charge and discharge rates with long cycle life while maintaining highly reversible capacity.

We fabricated the VO_2-graphene ribbons by a hydrothermal synthesis and chemical reduction procedure simultaneously (for details, see Experimental Methods). VO_2 has been long regarded as a promising electrode material for both organic and aqueous lithium ion batteries owing to its high capacity,

Received: January 1, 2013
Revised: March 4, 2013
Published: March 11, 2013

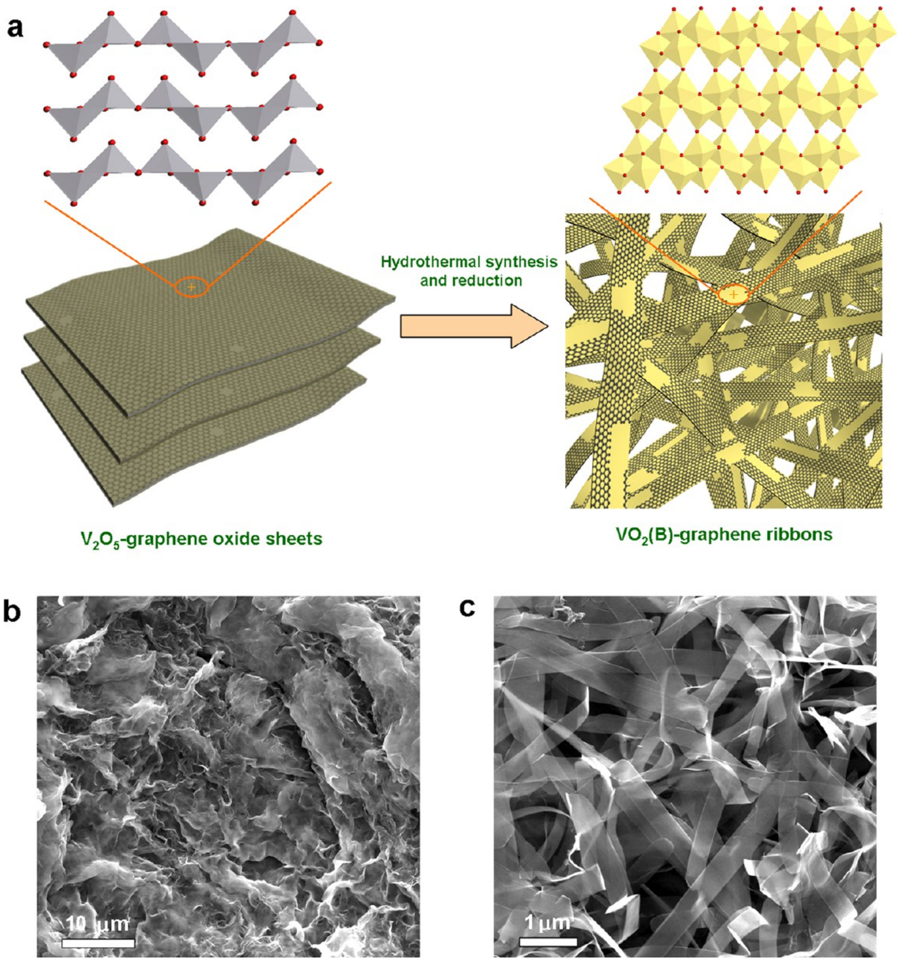

Figure 1. Synthesis of VO_2-graphene ribbons. (a) Fabrication of VO_2-graphene ribbons by a simultaneous hydrothermal synthesis and reduction of layered V_2O_5-graphite oxide composites at 180 °C. Structural model of layered, orthorhombic V_2O_5 phase projected along [001] facet is shown on the top left of part a. The ideal model of resulting monoclinic VO_2(B) phase projected along [010] facet is shown on the top right of part a, where the edge-sharing VO_6 octahedra are visible. Typical FE-SEM images of (b) V_2O_5-graphite oxide composites and (c) VO_2-graphene sample hydrothermally treated for 1.5 and 12 h, demonstrating the formation of numerous ribbons with the width of 200−600 nm and length of several tens of micrometers.

unique structure, and suitable electrode potential.[22−24] However it is limited by its poor cyclic performance as a result of its high charge-transfer resistance.[25] Our designed protocol involves the employment of graphene, which solves the electrical resistance problem with the VO_2 electrodes. To controllably fabricate the VO_2-graphene architectures, graphene oxide (GO) was used as the substrate for the in situ growth of VO_2 ribbons via the reduction of V_2O_5 by GO. This reaction was carried out at a constant temperate of 180 °C in a Teflon-lined autoclave, where V_2O_5 was initially dissolved in water and dispersed onto the surface of GO sheets and then gradually reduced to VO_2 ribbons (see Figure S1 in the Supporting Information). The resulting ribbons and residual graphene oxide sheets simultaneously became building blocks for the construction of 3D interpenetrating architectures. Notably, the contents of VO_2 ribbons in the as-prepared architectures were readily tunable by simply adjusting the ratio between V_2O_5 and GO during the synthesis process (three ratios of 9:1, 4:1, and 1.5:1 were chosen in this context). Finally, GO in the resulting samples was chemically reduced to graphene (reduced graphene oxide), giving rise to VO_2-graphene architectures with various VO_2 content (84%, 78%, and 68%) (Figure S2).

The as-prepared VO_2-graphene architectures, composed of numerous ribbons and sheets with 3D interpenetrating network, were observed by field emission scanning electron microscopy (FE-SEM) and transmission electron microscopy (TEM) (Figure 1c, 2a). The lateral sizes of these ribbon building blocks are typically in the ranges of 200−600 nm in width and several tens of micrometers in length (Figures 1c and 2a). Atomic force microscopy (AFM) images of the cross-section and thickness of the ribbons confirmed the same morphology as observed from SEM and TEM, having a uniform thickness of ~10 nm (Figure S3). Further inspection using high-resolution TEM (HRTEM) and the corresponding selected-area electron diffraction pattern (SAED) revealed that these ribbons are single crystalline, as seen by the well-defined crystalline lattices (Figure 2b−d). A typical HRTEM image (Figure 2c) discloses the lattice fringes with a spacing of 0.21 nm, in good agreement with the spacing of the (003) planes of VO_2 (B) (which is described as bilayers formed from edge-sharing VO_6 octahedra). More interestingly, the nanosheets are tightly covered with graphene layers, as confirmed by energy-dispersive X-ray (EDX) and electron energy-loss spectroscopy (EELS) (see Figure S4 in Supporting Information). Furthermore, the graphene layers decorating the VO_2 ribbons are not

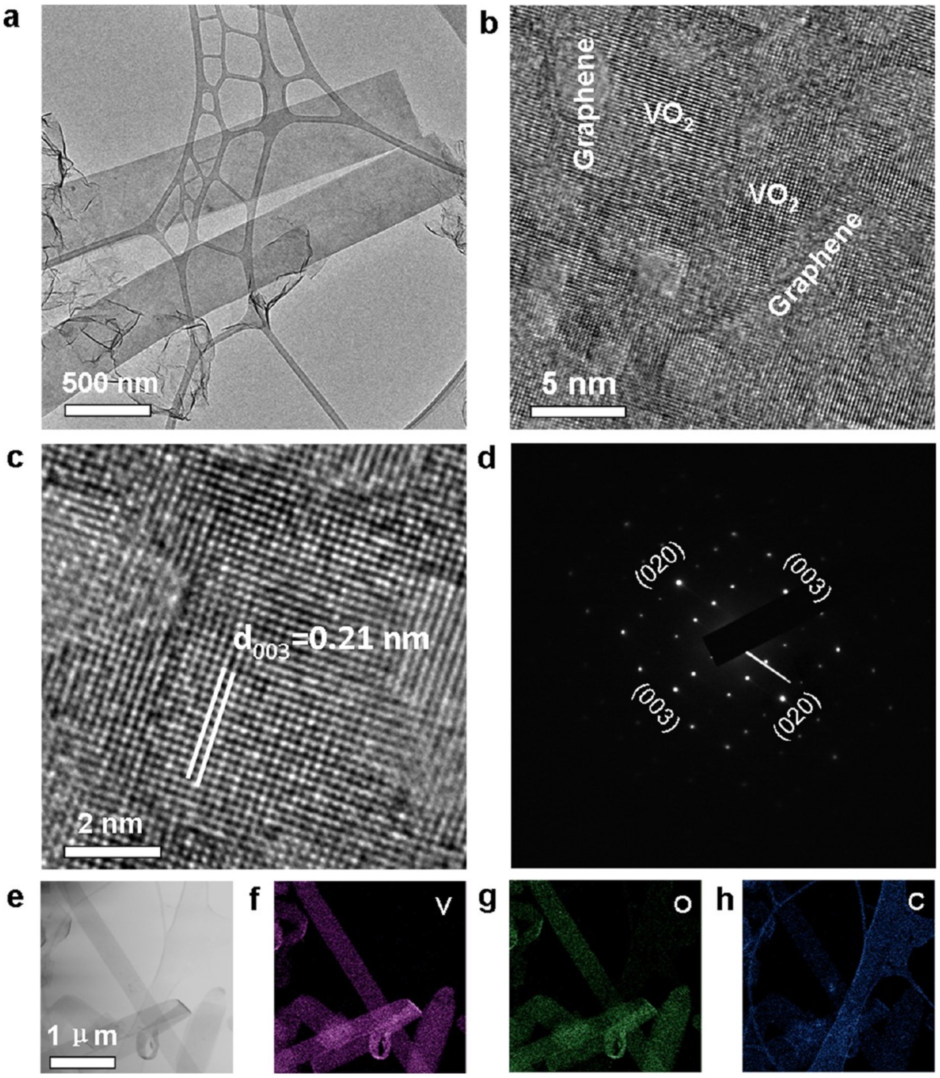

Figure 2. VO_2-graphene ribbons. (a) Typical TEM image and (b,c) HRTEM images of VO_2 ribbons show the incontinuous graphene layers on the surface of well-crystalline ribbons. The exposed lattice fringes shown in part c has a spacing of 0.21 nm, corresponding to the (003) plane of VO_2(B). (d) The representative diffraction patterns show well-defined arrays of dots, demonstrating the single crystalline feature of VO_2(B) ribbons. (e) Scanning transmission electron microscopy (STEM) image and corresponding elemental mapping of (f) vanadium, (g) oxygen, and (h) carbon, indicating the homogeneous dispersion of V, O, and C in all of the ribbons.

continuous (Figures 2b and S5). Such features are favorable for good compatibility with organic electrolytes and offer easy access for lithium ions as well as facilitation of the fast electron transfer, to promote lithium storage.

The structure of the ribbons is further analyzed by elemental mapping of vanadium, oxygen, and carbon. As presented in Figure 2e−h, vanadium, oxygen, and carbon atoms are homogeneously distributed in all of the ribbons. To gain further insight into the structure of the ribbons, we performed the X-ray diffraction (XRD) patterns, Raman, and X-ray photoelectron spectroscopy (XPS) analysis (Figures S6 and S7). The XRD patterns (Figure S6) are indexed in the space group $C2/m$ with standard lattice constants a = 12.03 Å, b = 3.693 Å, and c = 6.42 Å (β = 106.6°) for VO_2(B) with a monoclinic structure (JCPDS No. 31-1438).[24] Furthermore, no conventional stacking peak (002) of graphene sheets at 2θ = 26.6° is detected, suggesting that the residual graphene sheets may be individual monolayers that are homogeneously dispersed in the resulting 3D architectures. The XPS analysis (Figure S7a,c,d) further reveals that the atomic ratio between V and O is close to 1:2, very consistent with those from EDX and EELS. The porous nature of VO_2-graphene architectures is further demonstrated by the nitrogen physisorption measurements. Their adsorption−desorption isotherms exhibit a typical II hysteresis loop at a relative pressure between 0.6 and 0.9 (Figure S8), characteristic of pores with different pore sizes. Barrett−Joyner−Halenda (BJH) calculations disclose that the pore size distribution is in the range of 3−20 nm, except for the open macropores estimated from the SEM images. The adsorption data indicate specific surface areas of 405, 156, and 66 $m^2\ g^{-1}$ for the VO_2-graphene architectures with VO_2 contents of 68.3%, 78.1%, and 84.3%, respectively.

The electrochemical performances of the 3D VO_2-graphene architectures were systematically evaluated by galvanostatic discharge (lithium insertion)−charge (lithium extraction) measurements at various rates (nC), where nC corresponds to the full lithium extraction from electrodes in 1/n h. A very high reversible capacity of 415 mAh g^{-1} with stable cycle performance is achieved at 1C, in the case of VO_2-graphene architecture with the VO_2 content of 78% (Figure 3). This is in

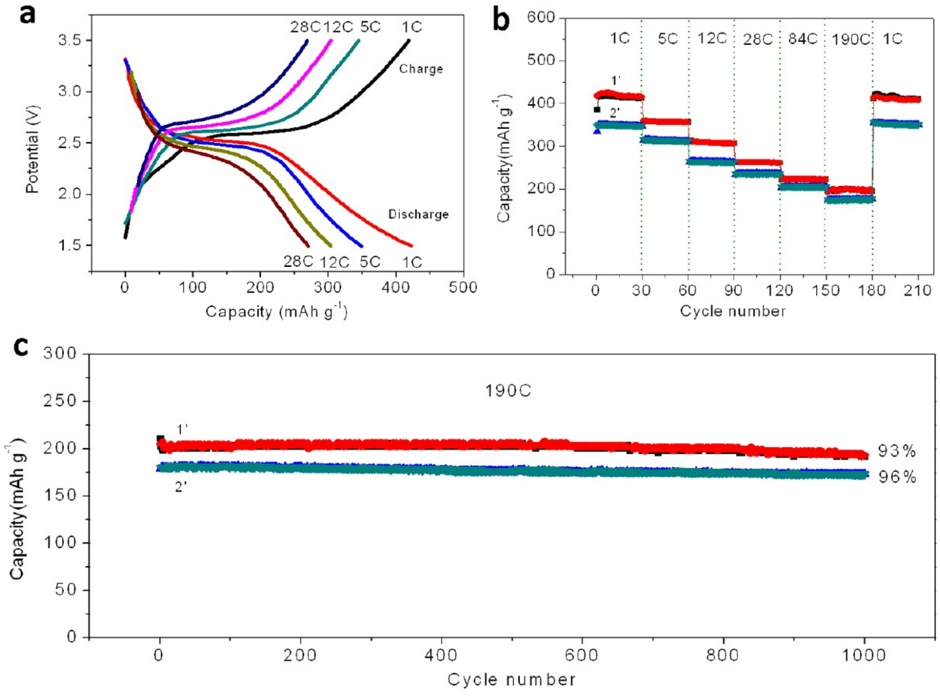

Figure 3. Electrochemical performance of VO_2-graphene architectures under room temperature. (a) Representative discharge−charge curves of VO_2-graphene (78%) architecture at various C-rates over the potential range of 1.5−3.5 V vs Li^+/Li. (b) Rate capacities of VO_2-graphene architectures with different VO_2 contents, measured for 30 cycles at each selected rate from 1C to 190C. (c) Capacity retentions of VO_2-graphene architectures when performing full discharge−charge at the highest rate of 190C (37.2 A g^{-1}) for 1000 cycles. 1′ and 2′ are denoted as VO_2-graphene architectures with the VO_2 contents of 78% and 68%, respectively.

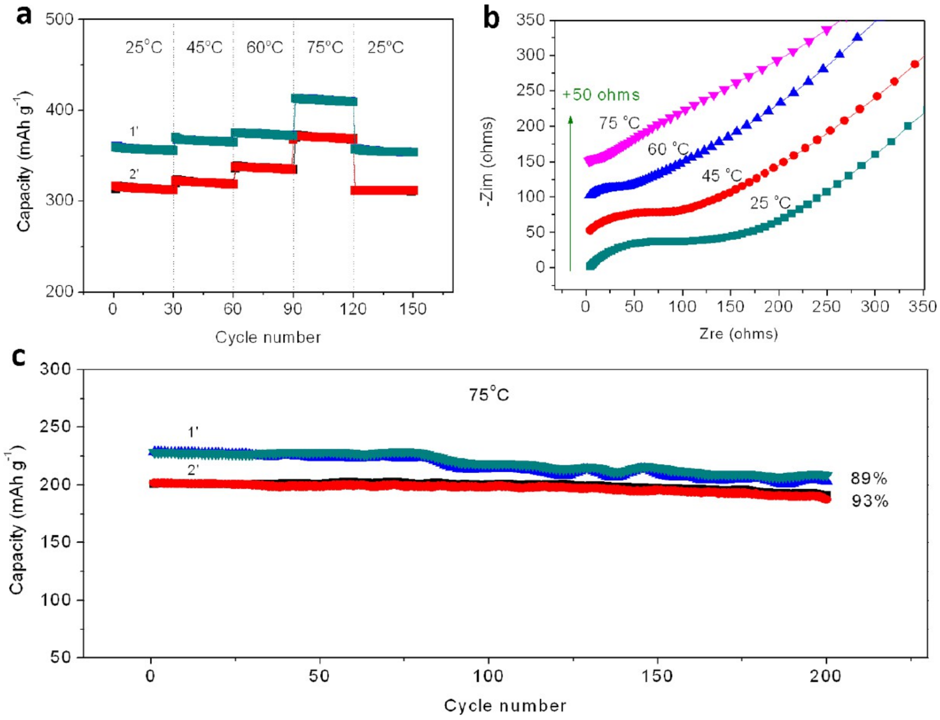

Figure 4. Electrochemical performance of VO_2-graphene architectures under various temperatures. (a) Cycle performance of VO_2-graphene architectures under various temperatures from 25 to 75 °C at a current rate of 5C (1.9 A g^{-1}) over the potential range of 1.5−3.5 V vs Li^+/Li. After the cycle performance test at 75 °C, the environmental temperature is recovered to 25 °C for another 30 cycles. (b) Nyquist plots of VO_2-graphene architecture (78%) after 30 cycles under various selected temperatures (25, 45, 60, and 75 °C), obtained by applying a sine wave with amplitude of 5.0 mV over the frequency range of 100 kHz to −0.01 Hz. (c) Capacity retentions of VO_2-graphene architectures under the highest temperature of 75 °C at a current rate of 28C. 1′ and 2′ are denoted as VO_2-graphene architectures with the VO_2 contents of 78% and 68%, respectively.

stark contrast to those reported for VO_2(B) nanomaterials, which show continuous and progressive capacity decay along with cycling processes.[23,25] Moreover, the initial reversible capacity is tunable by adjusting the content of VO_2 ribbons in the 3D architectures (Figures 3a and S9). The typical discharge−charge profiles (Figure 3a) further exhibit the classic potential plateaus of VO_2 (B) at ~2.5 and 2.6 V, corresponding to the formation of Li_xVO_2.[25] Although the electrode potentials are lower than those of the commercial cathode $LiCoO_2$, this is considered advantageous over high-power lithium ion batteries in regards to rapid discharge−charge rates commonly causing high polarization of the electrodes resulting in the oxidation and decomposition of the electrolyte; which couples with safety problems of batteries.[22,23]

More remarkably, the VO_2-graphene architectures exhibit ultrafast charging and discharging capability (Figures 3b, S9, and S10). For example, the VO_2-graphene architecture containing 78% VO_2 demonstrates reversible capacities as high as 222 and 204 mAh g^{-1} (Figure 3b) at the extremely high rates of 84C and 190C (corresponding to 43 and 19 s total discharge or charge), respectively. These high discharge−charge rates are 2 orders of magnitude greater than those currently used in lithium ion batteries. Moreover, even after 1000 cycles at the ultrahigh rate of 190C, both discharge and charge capacities are stabilized at about 190 mAh g^{-1}, delivering over 90% capacity retention (Figures 3c and S10). To the best of our knowledge, such an excellent high-rate performance is superior to all existing cathode materials reported for lithium ion batteries.

To understand why VO_2-graphene architectures exhibit such excellent rate performance, the solid-state diffusion time of lithium over VO_2 ribbons was estimated according to the formula of $t = L^2/D$.[10] A very short lithium diffusion time of less than 0.01 s is obtained on the basis of the average thickness of VO_2 ribbons (~10 nm) and the lithium diffusion coefficient in VO_2 ribbons (10^{-9}−10^{-10} cm^2 s^{-1}).[26] Clearly, the limiting factor for discharging and charging in our 3D architectures is the transfer of lithium ions and electrons to the surface of ribbons rather than the conventional solid-state diffusion, similar to supercapacitors. In addition to the favorable diffusion kinetics in VO_2-graphene architectures, the unique edge sharing structure of VO_2(B) can also be resistant to the lattice distortion and efficiently preserve the structural stability of VO_2(B) during long discharge−charge processes.[23] Hence, the ultrafast, supercapacitor-like charge and discharge rate having a long cycle life is achieved with VO_2-graphene architectures. Furthermore, at the ultrahigh rate of 190C, the specific powers are as high as 110 and 96 kW kg^{-1} for VO_2-graphene architecture having VO_2 contents of 78% and 68%, respectively. Assuming that the cathode takes up about 40% of the weight of a complete cell, these values are still 40 times higher than those of the current lithium ion batteries (~1 kW kg^{-1}).[1,27]

In the case of ultrafast charging and discharging, the electrochemical performance of an electrode material at high temperatures is another crucial factor. To assess the stability of our new material, we selected the aggressive tests where the electrodes were cycled under the temperatures of 25, 45, 60, and 75 °C, respectively (Figures 4, S11, and S12). Apparently, the capacity increases from 360 to 410 mAh g^{-1} with increasing temperature from 25 to 75 °C at a rate of 5C (Figure 4a). The enhanced capacity attributes to the significantly reduced contact and charge-transfer resistances in VO_2-graphene architecture under higher temperatures (see Figure 4b). At the highest temperature of 75 °C, our material still shows an excellent capacity retention of about 90% after 200 cycles at 28C (Figure 4c). In contrast, other reported cathodes commonly show large capacity decay under high temperatures even at the low rates (<1C).[28] These results clearly demonstrate that our cathode material can provide fast discharging and charging capability with high capacity and long cycle performance even at high temperatures. We believe that this is a breakthrough in cathode materials with ultrafast charging and discharging capability and can significantly prompt the rapid development and applications of high-power lithium ion batteries.

Experimental Methods. Graphene oxide (GO) nanosheets were synthesized from natural graphite flakes by a modified Hummers method, the details of which were described elsewhere.[20] 3D VO_2-graphene architectures were synthesized by a simultaneous hydrothermal synthesis and assembly procedure. In a typical procedure, a 10 mL of GO (2 mg mL^{-1}) aqueous dispersion was mixed with different amounts of commercially available V_2O_5 powder by sonication for 10 min. Then the resulting mixture was sealed in a Telfon-lined autoclave and was hydrothermally treated at 180 °C for various hours (1.5−24 h). No special definition, the samples were obtained at 12 h. Finally, the as-prepared samples were chemically reduced and freeze- or critical point-dried to preserve the 3D architectures formed during synthesis process.

The morphology and microstructure of the samples were systematically investigated by FE-SEM (JEOL 6500), TEM (JEOL 2010), HRTEM (Field Emission JEOL 2100), AFM (Digital Instrument Nanoscope IIIA), XPS (PHI Quantera X-ray photoelectron spectrometer), and XRD (Rigaku D/Max Ultima II Powder X-ray diffractometer) measurements. Nitrogen sorption isotherms and the Brunauer−Emmett−Teller (BET) surface area were measured at 77 K with a Quantachrome Autosorb-3B analyzer (USA). Electrochemical experiments were carried out in 2032 coin-type cells. The as-prepared VO_2-graphene monoliths or architectures were directly fabricated as binder/additive-free working electrodes by cutting then into small thin round slices with a thickness of ~1 mm and processing into these slices into thinner electrodes upon pressing. The area of the electrodes is 0.79 cm^{-2}. Pure lithium foil (Aldrich) was used as the counter electrode. The electrolyte consisted of a solution of 1m $LiPF_6$ in ethylene carbonate (EC)/dimethyl carbonate (DMC)/diethyl carbonate (DEC) (1:1:1 by volume) obtained from MTI Corporation. The cells were assembled in an argon-filled glovebox with the concentrations of moisture and oxygen below 0.1 ppm. The electrochemical performance was tested at various current rates in the voltage range of 1.5−3.5 V. The impedance spectra were recorded by applying a sine wave with amplitude of 5.0 mV over the frequency range from 100 kHz to 0.01 Hz.

■ ASSOCIATED CONTENT

Ⓢ Supporting Information

Additional information and figures. This material is available free of charge via the Internet at http://pubs.acs.org.

■ AUTHOR INFORMATION

Corresponding Author

*E-mail: sy13@rice.edu (S.Y.); ajayan@rice.edu (P.M.A.).

Author Contributions

S.Y. and Y.G. contributed equally to this work.

Notes

The authors declare no competing financial interest.

■ ACKNOWLEDGMENTS

This work was financially supported by U.S. Army Research Office through a MURI grant (W911NF-11-1-0362) on Novel Free-Standing 2D Crystalline Materials focusing on Atomic Layers of Nitrides, Oxides, and Sulfides. D.P.H. is grateful to the NSF for the Graduate Research Fellowship award grant no. 0940902. L.M. acknowledges the financial support provided by U.S. Office of Naval Research MURI grant (N000014-09-1-1066).

■ REFERENCES

(1) Kang, B.; Ceder, G. *Nature* **2009**, *458*, 190−193.

(2) Kang, K. S.; Meng, Y. S.; Breger, J.; Grey, C. P.; Ceder, G. *Science* **2006**, *311*, 977−980.

(3) Wu, H.; Chan, G.; Choi, J. W.; Ryu, I.; Yao, Y.; McDowell, M. T.; Lee, S. W.; Jackson, A.; Yang, Y.; Hu, L. B.; Cui, Y. *Nat. Nanotechnol.* **2012**, *7*, 309−314.

(4) Armand, M.; Grugeon, S.; Vezin, H.; Laruelle, S.; Ribiere, P.; Poizot, P.; Tarascon, J. M. *Nat. Mater.* **2009**, *8*, 120−125.

(5) Recham, N.; Chotard, J. N.; Dupont, L.; Delacourt, C.; Walker, W.; Armand, M.; Tarascon, J. M. *Nat. Mater.* **2010**, *9*, 68−74.

(6) Morcrette, M.; Rozier, P.; Dupont, L.; Mugnier, E.; Sannier, L.; Galy, J.; Tarascon, J. M. *Nat. Mater.* **2003**, *2*, 755−761.

(7) Jung, H. G.; Jang, M. W.; Hassoun, J.; Sun, Y. K.; Scrosati, B. *Nat. Commun.* **2011**, *2*, 516.

(8) Wang, H. L.; Yang, Y.; Liang, Y. Y.; Cui, L. F.; Casalongue, H. S.; Li, Y. G.; Hong, G. S.; Cui, Y.; Dai, H. J. *Angew. Chem., Int. Ed.* **2011**, *50*, 7364−7368.

(9) Zhang, H. G.; Yu, X. D.; Braun, P. V. *Nat. Nanotechnol.* **2011**, *6*, 277−281.

(10) Bruce, P. G.; Scrosati, B.; Tarascon, J. M. *Angew. Chem., Int. Ed.* **2008**, *47*, 2930−2946.

(11) Arico, A. S.; Bruce, P.; Scrosati, B.; Tarascon, J. M.; Van Schalkwijk, W. *Nat. Mater.* **2005**, *4*, 366−377.

(12) Chan, C. K.; Peng, H. L.; Liu, G.; McIlwrath, K.; Zhang, X. F.; Huggins, R. A.; Cui, Y. *Nat. Nanotechnol.* **2008**, *3*, 31−35.

(13) Lee, Y. J.; Yi, H.; Kim, W. J.; Kang, K.; Yun, D. S.; Strano, M. S.; Ceder, G.; Belcher, A. M. *Science* **2009**, *324*, 1051−1055.

(14) Magasinski, A.; Dixon, P.; Hertzberg, B.; Kvit, A.; Ayala, J.; Yushin, G. *Nat. Mater.* **2010**, *9*, 353−358.

(15) Ellis, B. L.; Makahnouk, W. R. M.; Makimura, Y.; Toghill, K.; Nazar, L. F. *Nat. Mater.* **2007**, *6*, 749−753.

(16) Poizot, P.; Laruelle, S.; Grugeon, S.; Dupont, L.; Tarascon, J. M. *Nature* **2000**, *407*, 496−499.

(17) Seo, J. W.; Jun, Y. W.; Park, S. W.; Nah, H.; Moon, T.; Park, B.; Kim, J. G.; Kim, Y. J.; Cheon, J. *Angew. Chem., Int. Ed.* **2007**, *46*, 8828−8831.

(18) Wang, H. L.; Cui, L. F.; Yang, Y. A.; Casalongue, H. S.; Robinson, J. T.; Liang, Y. Y.; Cui, Y.; Dai, H. J. *J. Am. Chem. Soc.* **2010**, *132*, 13978−13980.

(19) Bhardwaj, T.; Antic, A.; Pavan, B.; Barone, V.; Fahlman, B. D. *J. Am. Chem. Soc.* **2010**, *132*, 12556−12558.

(20) Yang, S. B.; Sun, Y.; Chen, L.; Hernandez, Y.; Feng, X. L.; Müllen, K. *Sci. Rep.* **2012**, *2*, 427.

(21) Taberna, L.; Mitra, S.; Poizot, P.; Simon, P.; Tarascon, J. M. *Nat. Mater.* **2006**, *5*, 567−573.

(22) Li, W.; Dahn, J. R.; Wainwright, D. S. *Science* **1994**, *264*, 1115−1118.

(23) Tsang, C.; Manthiram, A. *J. Electrochem. Soc.* **1997**, *144*, 520−524.

(24) Baudrin, E.; Sudant, G.; Larcher, D.; Dunn, B.; Tarascon, J. M. *Chem. Mater.* **2006**, *18*, 4369−4374.

(25) Zhao, Q. Q.; Jiao, L. F.; Peng, W. X.; Gao, H. Y.; Yang, J. Q.; Wang, Q. H.; Du, H. M.; Li, L.; Qi, Z.; Si, Y. C.; Wang, Y. J.; Yuan, H. T. *J. Power Sources* **2012**, *199*, 350−354.

(26) Rui, X. H.; Sim, D. H.; Xu, C.; Liu, W. L.; Tan, H. T.; Wong, K. M.; Hng, H. H.; Lim, T. M.; Yan, Q. Y. *RSC Adv.* **2012**, *2*, 1174−1180.

(27) Lee, S. W.; Yabuuchi, N.; Gallant, B. M.; Chen, S.; Kim, B. S.; Hammond, P. T.; Shao-Horn, Y. *Nat. Nanotechnol.* **2010**, *5*, 531−537.

(28) Sun, Y. K.; Myung, S. T.; Park, B. C.; Prakash, J.; Belharouak, I.; Amine, K. *Nat. Mater.* **2009**, *8*, 320−324.